Measurement of double-differential neutron yields for iron, lead, and bismuth induced by 107-MeV protons for research and development of accelerator-driven systems

Hiroki Iwamoto[1,*], *Keita* Nakano[1], *Shin-ichiro* Meigo[1], *Daiki* Satoh[1], *Yosuke* Iwamoto[1], *Kenta* Sugihara[2], *Katsuhisa* Nishio[1], *Yoshihiro* Ishi[3], *Tomonori* Uesugi[3], *Yasutoshi* Kuriyama[3], *Hiroshi* Yashima[3], *Kota* Okabe[1], *Hiroyuki* Makii[1], *Kentaro* Hirose[1], *Riccardo* Orlandi[1], *Fumi* Suzaki[1], *Akito* Oizumi[1], *Kazuaki* Tsukada[1], *Fujio* Maekawa[1], and *Yoshiharu* Mori[3]

[1]Japan Atomic Energy Agency (JAEA), Tokai-mura, Ibaraki, Japan
[2]High Energy Accelerator Organization (KEK), Tsukuba, Ibaraki, Japan
[3]Kyoto University, Kumatori-cho, Osaka, Japan

Abstract. For the research and development of accelerator-driven systems (ADSs) and fundamental ADS reactor physics research using the Kyoto University Critical Assembly combined with the fixed-field alternating gradient (FFAG) accelerator, we are conducting a series of experiments on double-differential neutron yields using the FFAG accelerator at Kyoto University. This paper presents an overview of the experiments together with preliminary results.

1 Introduction

Spallation neutrons play an important role in the research and development of accelerator-driven systems (ADSs) [1]. In the framework of the fundamental research on the ADSs, many reactor physics experiments on the ADS have been performed using the Kyoto University Critical Assembly combined with the fixed-field alternating gradient (FFAG) accelerator at Kyoto University [2–4]. To examine details of the experimental results, in-depth information about spallation neutrons produced by the bombardment of spallation targets with the FFAG proton beam is required.

In this study, we measured the proton-induced double-differential neutron yields for the important materials of the ADS beam window and spallation target (i.e. Fe, Pb, and Bi) using two different thickness of targets, namely the thick target neutron yields (TTNYs) and the neutron-production double-differential cross sections (DDXs), with the time-of-flight (TOF) method. The obtained TTNY and DDX data were compared with the particle transport calculation results by the particle and heavy-ion transport code system (PHITS) [5] using the Monte Carlo-based spallation models (i.e. the Liège intranuclear cascade model Version 4.6 (INCL4.6) [6], the Bertini intranuclear cascade (INC) model [7], and the JAERI quantum molecular dynamics model (JQMD) [8], which were coupled with the generalized evaporation model (GEM) [9]).

This paper presents an overview of the TTNY and DDX measurements including preliminary DDX results. Details of the TTNY measurement and its important results can be seen in Iwamoto, et al [10].

2 Experiment and data analysis

The experiment was performed at the experimental hall of the Innovation Research Laboratory in the Institute for Integrated Radiation and Nuclear Science, Kyoto University. Figure 1 shows the horizontal plane view of the experimental setups for the TTNY and DDX measurements. Figure 2 shows a schematic of the targets and vacuum chambers used for the TTNY and DDX measurements. For each measurement, the target installed in the vacuum chamber was bombarded with a proton beam accelerated to 107 MeV with the beam width of <10 ns (1σ) and the repetition rate of 30 Hz using the FFAG accelerator. The proton beam profile was monitored using a fluorescent plate and a compact coupled device camera before the TTNY and DDX measurements.

The characteristics of the targets used are listed in Tables 1 and 2, where the ranges and energy losses for the 107-MeV protons were estimated using the Bethe–Bloch formula. As target materials for the TTNY measurements, 30-mm-thick Fe, Pb, and Bi (chemical purity > 99.999%) were employed, which are thick enough to stop 107-MeV protons in these materials. While thinner targets are better from the standpoint of the DDX measurements, this study employed 2-mm-thick Pb and 5-mm-thick Bi for the sake of statistics. The diameter of each target was 48 mm such that almost all the protons hit the target.

To achieve good statistics and wide-scope neutron energy spectrum measurement, we developed a neutron de-

*e-mail: iwamoto.hiroki@jaea.go.jp

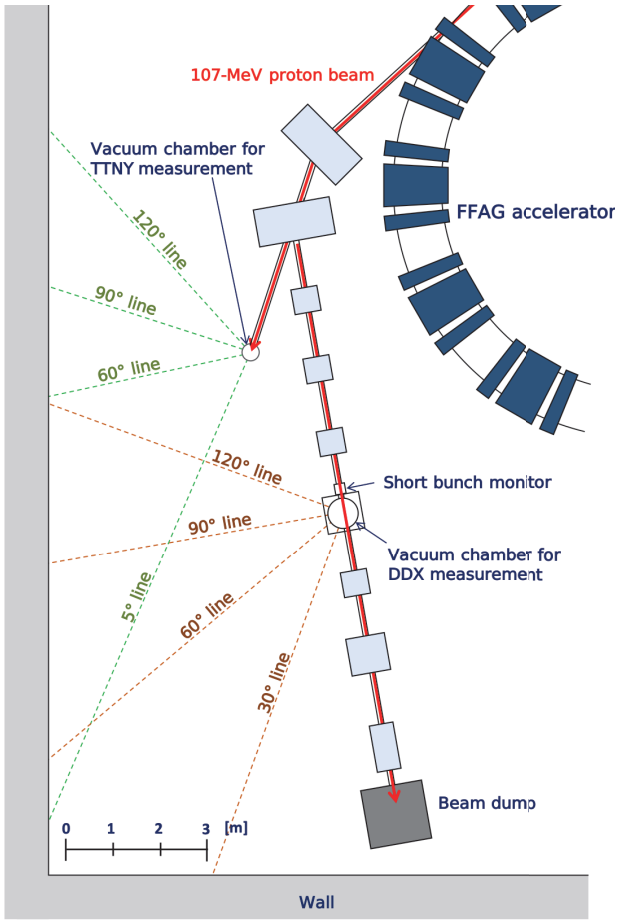

Figure 1. Horizontal plane view of the experimental setup.

Table 1. Targets used in the TTNY measurement

Target	Dimension	Range [mm]
Fe	∅48 mm × 30 mm-t	16.1
Pb	∅48 mm × 30 mm-t	15.9
Bi	∅48 mm × 30 mm-t	18.5

Table 2. Targets used in the DDX measurement

Target	Dimension	Energy loss [MeV]
Pb	∅48 mm × 2 mm-t	7.97
Bi	∅48 mm × 5 mm-t	18.0

tector system comprising eight neutron detectors; each detector includes a small EJ-301 liquid organic scintillator (8 mm in diameter and 20 mm in depth) and a photomultiplier tube (PMT). Figure 3 shows the neutron detector system. In the TTNY measurement, a 16-mm-thick Cu block was placed in front of them to prevent scattered protons from entering the EJ-301 scintillators. In the DDX measurement, a VETO counter composed of a plastic scintillator (W110 mm × H110 mm × 2 mm-t) with a light guide and PMT was placed in front of the neutron detectors to remove the charged particle events. Using this system, spallation neutrons produced from the target were detected at a distance of several meters from the target at several de-

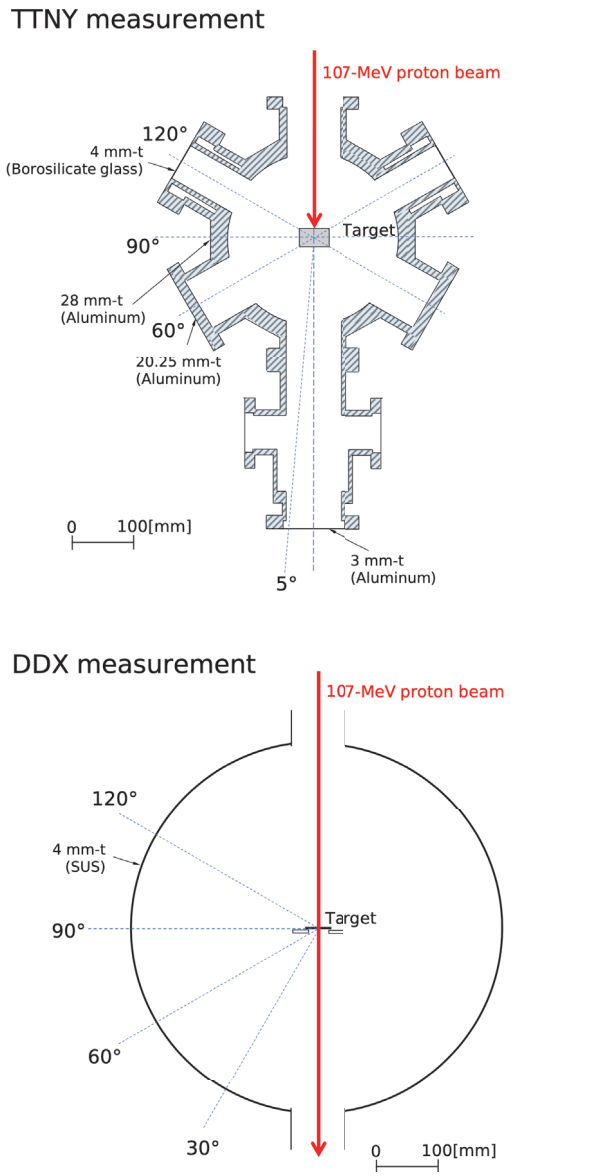

Figure 2. Horizontal view of the targets installed in the vacuum chambers for the TTNY (top) and DDX (bottom) measurements.

tector angles from the beam axis (Figure 1). Table 3 summarizes the flight path length for the experiment.

The corresponding neutron detectors were connected to the input terminals of a multi-channel digitizer (SIS3316 desktop digitizer) with Field-Programmable Gate Arrays (FPGAs). Analog charge signals transmitted from PMTs were converted to 14-bit digital signals using analog-to-digital converters (ADCs), and the signal charges integrated over specific two gate widths (i.e. fast and slow gates) were recorded using the ADC FPGAs. The data recorded were transmitted from the gigabit Ethernet to a personal computer using the internet protocol. Logic signals used as start signals were obtained from a 30-Hz radio frequency trigger of the FFAG accelerator via a constant fraction discriminator.

The light outputs of neutron detectors in the unit of electron equivalent (ee) were calibrated for two threshold

Table 3. Detector angles and flight path lengths in the TTNY and DDX measurements

	Detector angle [°]	Flight path length [m] Fe	Pb	Bi
TTNY meas.	5	5.41	5.42	5.32
	60	1.98	2.71	2.98
	90	—	2.48	2.47
	120	4.24	4.50	4.35
DDX meas.	30	—	7.24	—
	60	—	6.19	6.19
	90	—	3.93	4.05
	120	—	3.75	4.89

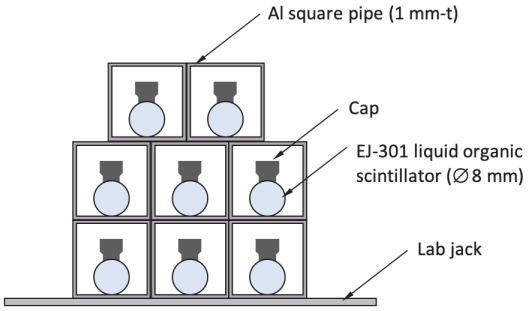

Figure 3. Front view of the neutron detector system.

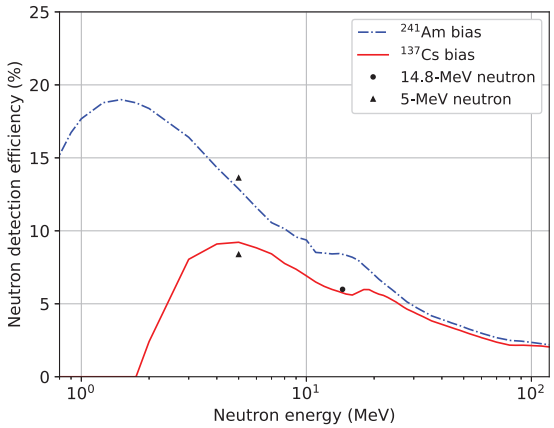

Figure 4. Neutron detection efficiency of the EJ-301 liquid organic scintillator for the ^{241}Am and ^{137}Cs biases calculated based on the SCINFUL mode of the PHITS. The black circle and triangles indicate our data measured using 5-MeV and 14.8-MeV monoenergetic neutrons at the Facility of Radiation Standards (FRS), JAEA [12].

levels: a photo-peak of 60-keV gamma-rays emitted from ^{241}Am (60 keVee, hereafter its bias is referred to as ^{241}Am bias) and the Compton edge induced by 662-keV gamma-rays from ^{137}Cs (483 keVee, hereafter its bias is referred to as ^{137}Cs bias). The room scattering neutrons were measured using a shadow bar composed of stainless steel (W50 mm × H50 mm × D1000 mm) and subtracted from the measured data without the shadow bar. To prevent background neutrons due to the FFAG septum magnet (and the proton beam dump for the DDX measurement) from entering the neutron detector system, the system was shielded using Fe and concrete blocks of several tens of centimeters in the actual experiments. Each measurement time ranged from 1 to 3 h.

The detected neutron and gamma-ray events were discriminated by the pulse shape discrimination method. The neutron energy spectra were obtained from the neutron TOF spectra based on relativistic kinematics. The TTNY and DDX were derived using the following equations:

$$\frac{\mathrm{d}^2 Y}{\mathrm{d}u\,\mathrm{d}\Omega} = \frac{N_\mathrm{n}}{\Delta u\,\Delta\Omega}\frac{1}{N_\mathrm{p}\,\epsilon(E_\mathrm{n})\,\eta(E_\mathrm{n})} \quad (1)$$

and

$$\frac{\mathrm{d}^2 \sigma}{\mathrm{d}E_\mathrm{n}\,\mathrm{d}\Omega} = \frac{N_\mathrm{n}}{\Delta E_\mathrm{n}\,\Delta\Omega}\frac{1}{N_\mathrm{p}\,N_\mathrm{t}\,\epsilon(E_\mathrm{n})\,\eta(E_\mathrm{n})}, \quad (2)$$

where $N_\mathrm{n}/\Delta u\Delta\Omega$ is the number of neutrons detected at the lethargy bin size Δu and the solid angle at the detector position $\Delta\Omega$; $N_\mathrm{n}/\Delta E_\mathrm{n}\Delta\Omega$ is the number of neutrons detected at the energy bin size E_n and $\Delta\Omega$; N_p is the number of incident protons, which was deduced based on the monitored beam current and measurement time; ϵ is the neutron detection efficiency of the EJ-301 liquid organic scintillator, which was obtained from the calculation results using the SCINFUL mode of the PHITS [11] (Figure 4); and η is the neutron attenuation/amplification ratio from the target to the neutron detector system, which was obtained from a Monte Carlo transport calculation results using the PHITS.

3 Results and discussion

Figure 5 compares the neutron energy spectra of the 107-MeV proton-induced TTNYs and DDXs at a detector angle of 120° between the measured and calculation results. Note that the measured DDX data are preliminary results, which need more investigation on experimental uncertainty. The neutron energy spectra at energies of >0.7 MeV were successfully obtained using the developed neutron detector and data acquisition (DAQ) system.

It is observed from Figure 5 that, the spallation models have specific trends at emission angle of 120°, and these trends are common to both TTNYs and DDXs. The JQMD model apparently overestimates the energy spectra at energies from 10 to 30 MeV. As discussed in Ref. [10], this overestimation would be resolved by modifying the so-called switching parameter in JQMD, which is an adjustable parameter to switch the calculation of the pre-equilibrium and evaporation processes. The Bertini INC model underestimates the energy spectra for all the cases. This trend is similar to the results obtained by our previous experimental study using a mercury target irradiated with a 3-GeV proton beam [13]. The INCL4.6 model overall agrees with experimental data, while underestimation is seen at ~10 MeV. The JENDL-4.0/HE reproduces spectrum shapes reasonably, but it overestimates the evaporation neutron spectra at energies of <10 MeV.

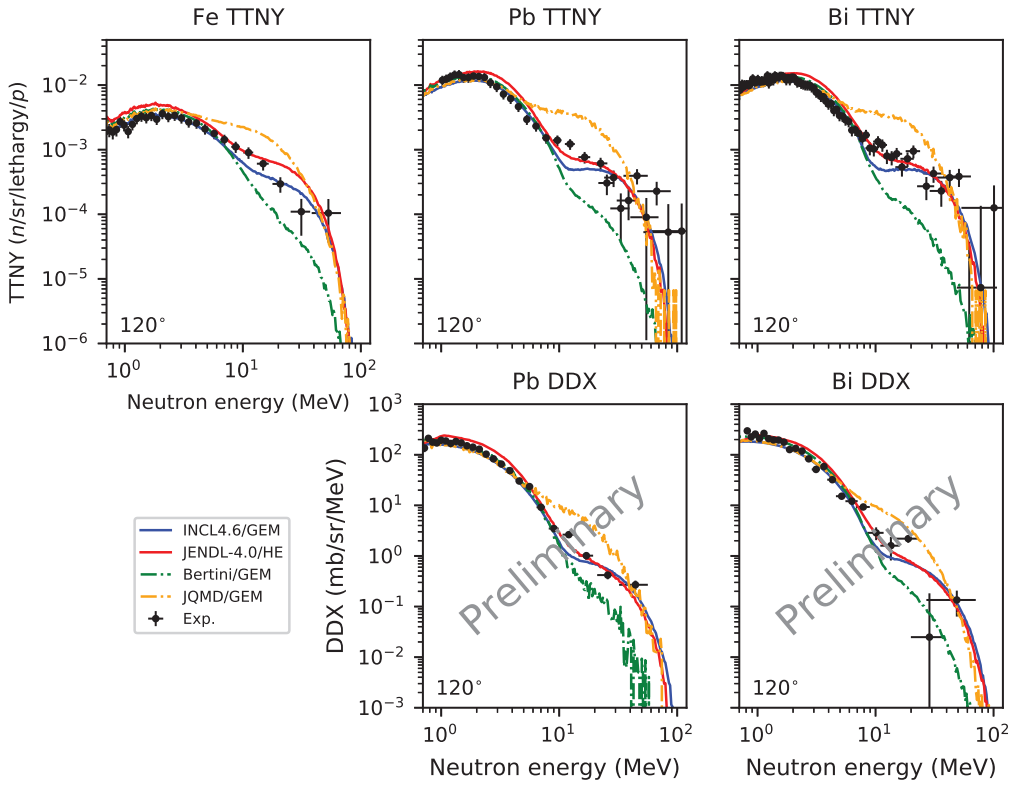

Figure 5. Proton-induced TTNYs at 120° for Fe, Pb, and Bi (top panels) and DDXs at 120° for Pb and Bi (bottom panels).

4 Conclusion

We measured the 107-MeV proton-induced double-differential TTNYs for Fe, Pb, and Bi and neutron production DDXs for Pb and Bi with the TOF method using the FFAG accelerator at Kyoto University. The neutron energy spectra of TTNYs and DDXs were successfully obtained using the developed neutron detector and DAQ system. We found characteristic trends of the respective spallation model calculations for the obtained neutron energy spectra. Further work is needed to determine the trend of the discrepancy between the experimental and calculation results. We are conducting a detailed data analysis for the DDX measurement. We expect that our experimental study will contribute to the research and development of the ADS and help improve the spallation models in the incident energy range of ~100 MeV.

Acknowledgements

This study was supported by MEXT Innovative Nuclear Research and Development Program under Grant No. JPMXD0219214562. The authors would like to express their gratitude to Dr. Daisuke Maki and Prof. Yuichi Oki of Kyoto University for their support during the experiment.

References

[1] T. Sugawara et al., Prog. Nucl. Energy **106**, 27–33 (2018)
[2] C.H. Pyeon et al., J. Nucl. Sci. Technol. **46**(12), 1091–1093 (2008)
[3] Y. Mori et al., Proc. of the international particle accelerator conference (IPAC2011) Sep. 4–9, 2011; San Sebàstian, Spain
[4] H. Iwamoto et al., J. Nucl. Sci. Technol. **54**(4), 432–443 (2017)
[5] T. Sato et al., J. Nucl. Sci. Technol **55**(6), 684–690 (2022)
[6] A. Boudard et al., Phys. Rev. C **87**, 014606 (2013)
[7] H.W. Bertini, Phys. Rev. **188**, 1711 (1969)
[8] K. Niita et al., Phys. Rev. C **52**, 2620–2635 (1995)
[9] S. Furihata et al., Nucl. Instrum. Methods Phys Res **B171**, 251–258 (2000)
[10] H. Iwamoto et al., J. Nucl. Sci. Technol. (Published online, 2022), DOI: 10.1080/00223131.2022.2115423
[11] D. Satoh et al., J. Nucl. Sci. Technol. **59**(8), 1047–1060 (2022)
[12] Y. Tanimura et al., Prog. Nucl. Sci. Technol **4**, 388–391 (2014)
[13] H. Matsuda et al., Nucl. Instrum. Methods Phys Res **B483**, 33–40 (2020)